The synthesis of copper-modified biochar from *Elsholtzia Harchowensis* and its electrochemical activity towards the reduction of carbon dioxide

Shiqi Chen, Wei Liu, Ziwei Mei, Haifu Li, Wenyu Zhao, Junkai Zhao and Hong Tao*

Department of Environmental Science and Engineering, University of Shanghai for Science and Technology, Shanghai, China

Phytoremediation techniques have been widely used in the treatment of heavy metal contaminated soils in recent years, but there is no effective post-treatment method for plant tissues containing heavy metals after remediation. *Elsholtzia Harchowensis* is a copper hyperaccumulator, commonly distributed in copper mining areas and often used for soil remediation of mine tailings. Moreover, copper-based catalysts are widely used in electrocatalytic reduction of carbon dioxide, which aims to convert carbon dioxide into useful fuels or chemicals. In this study, copper-modified biochar was prepared from *Elsholtzia Harchowensis*. Its specific surface area can reach as high as 1202.9 m^2/g, with a certain porous structure and even distribution of copper on the amorphous carbon. Various products (such as carbon monoxide, methane, ethanol, and formic acid) could be obtained from the electrolytic reduction of carbon dioxide by using the as-prepared catalyst. Instantaneous current density of up to 15.3 mA/cm^2 were achieved in 1.0 M $KHCO_3$ solution at a potential of -0.82 V (vs. RHE). Electrolysis at a potential of -0.32 V (vs. RHE) for 8 h resulted in a stable current of about 0.25 mA/cm^2, and the Faraday efficiency (FE) of carbon monoxide can reach as high as 74.6%. In addition, electrolysis at a potential of -0.52 V (vs. RHE) for 8 h led to a stable current of about 2.2 mA/cm^2 and a FE of 8.7% for the C_2 product. The rich variety of elements in plants leads to catalysts with complex structural and elemental characteristics as well, which facilitates the electrolytic reduction of carbon dioxide with a variety of useful products.

KEYWORDS

Elsholtzia Harchowensis, biochar, electrocatalysis, CO_2RR, carbon-based materials

1 Introduction

In recent years, heavy metal pollution in soil has attracted more and more attention, mainly including copper (Cu), zinc (Zn), chromium (Cr), cadmium (Cd), lead (Pb), mercury (Hg), arsenic (As) and nickel (Ni). The soil was contaminated with industrial and agricultural activities, resulting in much higher heavy metal content than the natural background value and leading to ecological degradation and soil quality deterioration (Adrees et al., 2015; Sarwar et al., 2017). China has very rich reserves of mineral resources, but due to improper mining methods and other problems, the problem of

heavy metal pollution of soil caused by mining is becoming increasingly prominent. Phytoremediation is an emerging environment-friendly remediation technology, which has a wide remediation area, low cost, small disturbance to soil, convenient operation and simple management, and no secondary pollution. Furthermore, it increases the vegetation cover of the mining area, which can effectively protect the surface soil and reduce soil erosion, and has important practical significance and strong operability for the ecological restoration of the soil around the mining area and the abandoned land of the mining area as well as the remediation of the heavy metal contaminated soil in the mining area (Alvarenga et al., 2009; Grandlic et al., 2009; Barceló and Poschenrieder, 2011; Rascio and Navari-Izzo, 2011).

Elsholtzia Harchowensis, commonly known as copper grass flower, is an annual herb in the family *Labiatae*, which can grow in soils with high copper content and is regarded as an indicator plant for copper mines. The plant has been applied in the field of environmental pollution management, mine site revegetation, plant mineral search and tolerance mechanism to heavy metals (Song et al., 2003; Jian et al., 2004; Jiang et al., 2004). Nowadays, *Elsholtzia Harchowensis* is one of the main remediation plants for copper-contaminated soils in China, and post-treatment of plant tissues containing heavy metals is a key problem to be solved, as it is very likely to cause secondary contamination if not handled properly (Li et al., 2020). In Tongling City, the total area of the mine is estimated to be around 2,688 hectares, and the phytoremediation treatment area is up to 1000 ha. The area has adopted *Elsholtzia Harchowensis* to remediate the soil contaminated by the mine, with 5.3 ha of *Elsholtzia Harchowensis* planted around the tailings pond alone, producing a large number of plants containing the heavy metal copper. Due to the low copper content, the economic benefits of incineration to recover copper are not obvious. The current treatment methods still focus on combustion and composting, which can cause secondary pollution to the air and soil. Therefore, how to effectively treat these plant tissues containing heavy metal copper has become a great challenge.

On the other hand, with the rapid development of industry, CO_2 emissions have increased significantly, seriously disrupting the carbon cycle and even the balance of the entire ecosystem in the Earth's environment (Wang et al., 2011). As a greenhouse gas, the utilization of CO_2 contributes to sustainable economic and social development, and its conversion into fuels or chemicals with high added value can not only alleviate the energy crisis (Sun et al., 2021; Niu et al., 2022), but also achieve a closed carbon cycle and mitigate the greenhouse effect (Mac Dowell et al., 2017; Birdja et al., 2019; Tang et al., 2021). Various strategies (such as electrocatalytic reduction (Costentin et al., 2013; Qiao et al., 2014; Nitopi et al., 2019; Ross et al., 2019), thermocatalytic hydrogenation (Markewitz et al., 2012), photoelectrocatalysis (Fu et al., 2012; Habisreutinger et al., 2013) etc.) are investigated in the past decades for the conversion of CO_2 to useful products. Among those methods, electrocatalytic reduction of CO_2 enables both renewable electricity storage and direct conversion of CO_2 into value-added products such as CH_4, C_2H_4, C_2H_5OH, and $HCOOH$ (Hori, 2008; Franco et al., 2020; Zhang et al., 2023).

In the electrocatalytic CO_2RR studied so far, the non-precious metal Cu has attracted much attention because of its unique catalytic properties (Chen et al., 2021; Chen et al., 2022b). Cu materials are cheap and exhibit unique catalytic properties in electrocatalytic CO_2

reduction reactions, producing a wide range of hydrocarbons and alcohols with high current efficiencies. For instance, CO_2 could be electrochemically reduced to CH_4 and C_2H_4 on the surface of metallic Cu as reported by Hori et al. (Hori et al., 1986; Zhu et al., 2013). Among all the reduction products of CO_2RR, multi-carbon (C_2^+) products, such as ethylene and ethanol, have a higher energy density as well as additional commercial utilization value. In addition, high overpotential is needed to achieve large current density as well as fast reaction rate for CO_2 conversion, which enhances the hydrogen evolution reaction (HER) at the same time. To solve this problem as well as to improve the selectivity of specific products, novel electrodes have been developed recently such as bimetallic materials (Au-Cu (Zheng et al., 2018), Ag-Cu (Fu et al., 2022), Pd-Cu (Costentin et al., 2014)), molecular sieve catalysts (Liu et al., 2018), carbon based materials (Wang et al., 2017; Liu et al., 2022), and transition metal single-atom catalysts (SACs) (Wang et al., 2018; Sun et al., 2021; Chen et al., 2022a) etc.

Carbon based materials have attracted more and more attention world widely due to simple preparation method, low cost, high catalytic ability and stability (Wang et al., 2021). Recently, heteroatom doping has been considered an effective strategy for improving electrocatalytic performance (Asefa, 2016; Wang et al., 2019; Zhang et al., 2019; Liu et al., 2023). For carbon materials, S dopant has been proved to be able to adsorb the generated H* at reduction potential and promote the dissociation of water, so it has attracted extensive attention of many researchers (Ma et al., 2019; Sun et al., 2020; Zheng et al., 2021). Biochar material is a good carrier with electrical conductivity and can be modified by doping to obtain electrocatalysts with large specific surface area and highly dispersed active components, which have broad application prospects. In this study, *Elsholtzia Harchowensis* collected in Tongling, China, was used to prepare carbon-based catalytic materials from copper-containing biomass. Exploring the use of copper accumulated in plant cells for electrocatalytic conversion of carbon dioxide is expected to utilize waste *Elsholtzia Harchowensis* and obtain considerable benefits for the environment. The modified biochar was prepared by carbonization at high temperature and then activation by KOH. The differences in the electrocatalytic performances of biochar prepared by untreated *Elsholtzia Harchowensis* and $CuSO_4$ soaked plant tissues were compared. Since the sulfur-doped Cu-based biochar was obtained by soaking the $CuSO_4$ solution-treated material and introducing both Cu and S into it, the influence and correlation of non-metallic elements on its performance and structure for electrocatalytic reduction of CO_2 were also investigated in this study.

2 Experimental

2.1 Experimental reagents and materials

Copper sulfate pentahydrate ($CuSO_4 \cdot 5H_2O$, AR), potassium hydroxide (KOH, AR), anhydrous sodium sulfate (Na_2SO_4, AR), anhydrous ethanol (CH_3CH_2OH, AR), potassium bicarbonate ($KHCO_3$, AR) were purchased from Sinopharm Chemical Reagent Co., Ltd. Nafion solution (5% D520) was purchased from Suzhou Yilongsheng Energy Technology Co., Ltd. All reagents were of analytical grade and were used as received
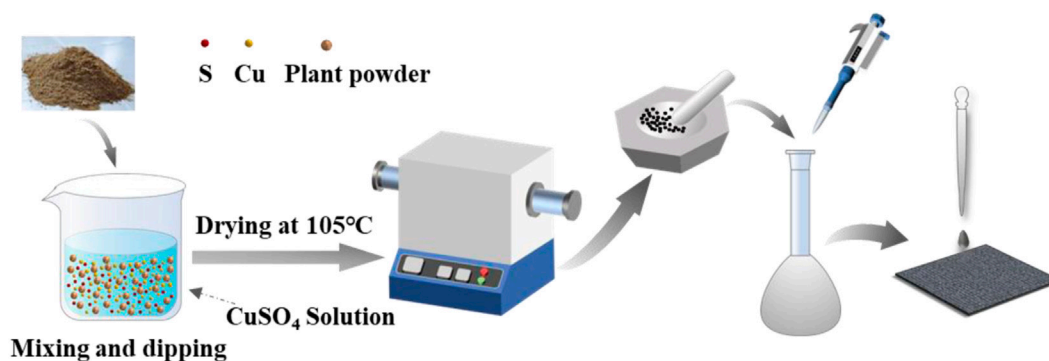
FIGURE 1
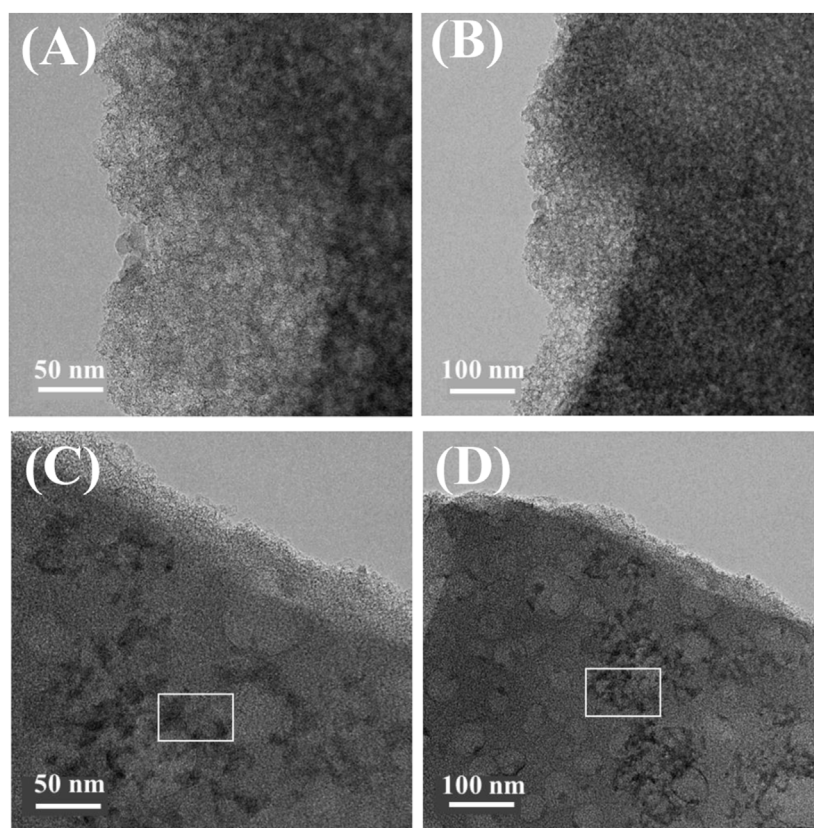Schematic diagram of the preparation of Cu/C-S electrode material.

FIGURE 2
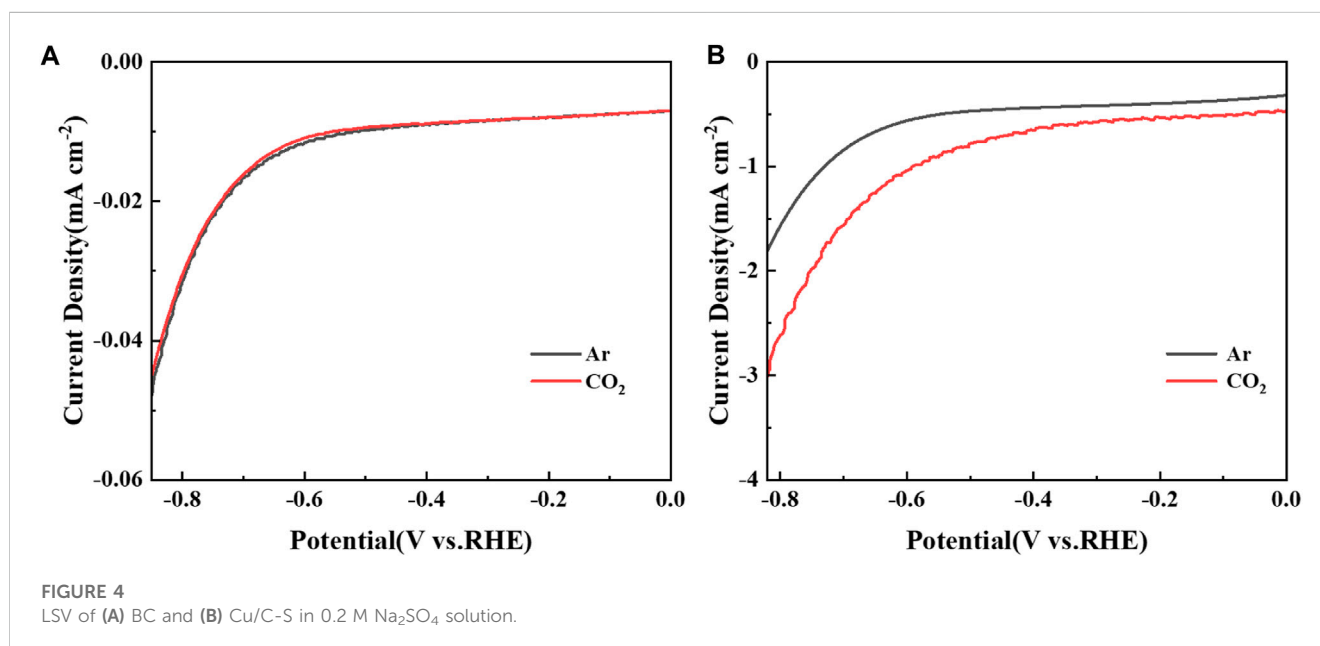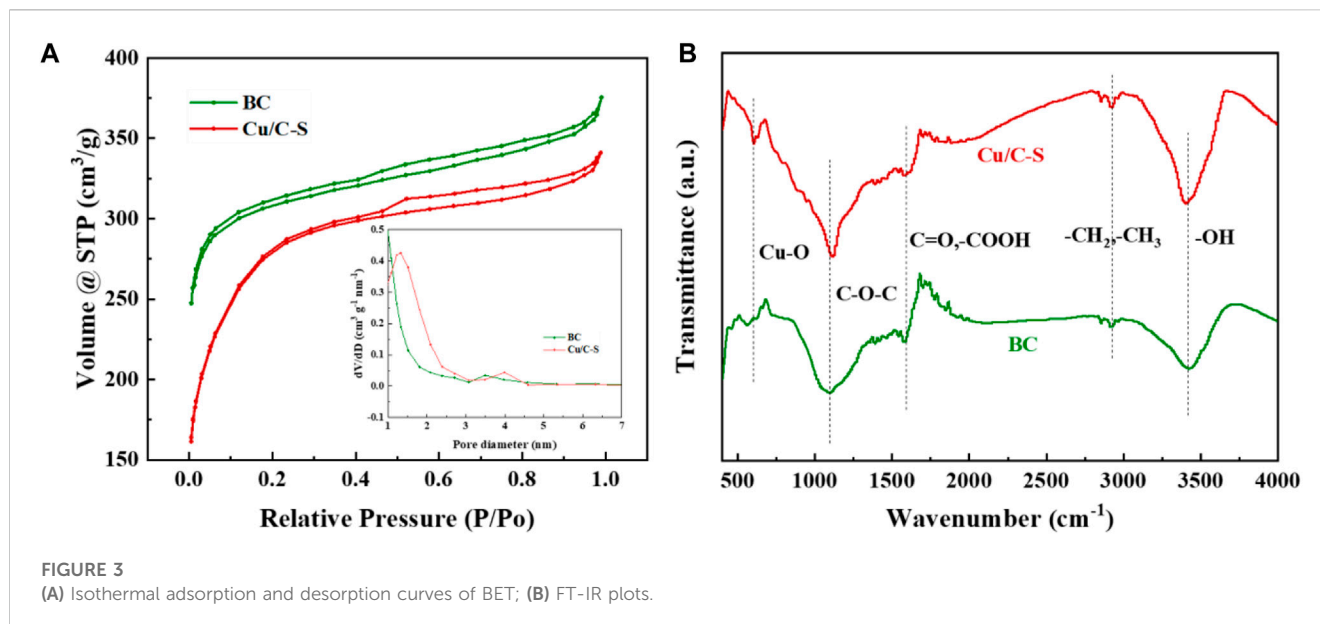TEM images of BC and Cu/C-S materials: **(A)** and **(B)**: BC; **(C)** and **(D)**: Cu/C-S.

without further purification. *Elsholtzia Harchowensis* was collected from the copper mine area of Tongling City, Anhui Province, China.

2.2 Preparation of catalysts

2.2.1 Biochar (BC)

The collected *Elsholtzia Harchowensis* was cleaned, dried and crushed after sampling, and then a 40 mesh sieve was used to obtain powdered plant tissue. Carbonization was performed in a tube furnace under specific conditions of nitrogen atmosphere, with a heating rate of 2 °C/min to 700 °C, and maintained for 90 min. After cooling, the samples were ground and processed. Potassium hydroxide powder was added at a mass ratio of 1:4 (carbon: KOH) and mixed thoroughly, after which the mixture was placed again in a tube furnace at a heating rate of 2 °C/min to 700 °C under a nitrogen atmosphere for 90 min to obtain activated biochar material (Abbas et al., 2022). After cooling, the sample was washed with pure

FIGURE 3
(A) Isothermal adsorption and desorption curves of BET; **(B)** FT-IR plots.

FIGURE 4
LSV of **(A)** BC and **(B)** Cu/C-S in 0.2 M Na_2SO_4 solution.

water until neutral, dried, and ground in an agate bowl to obtain pristine biochar (BC).
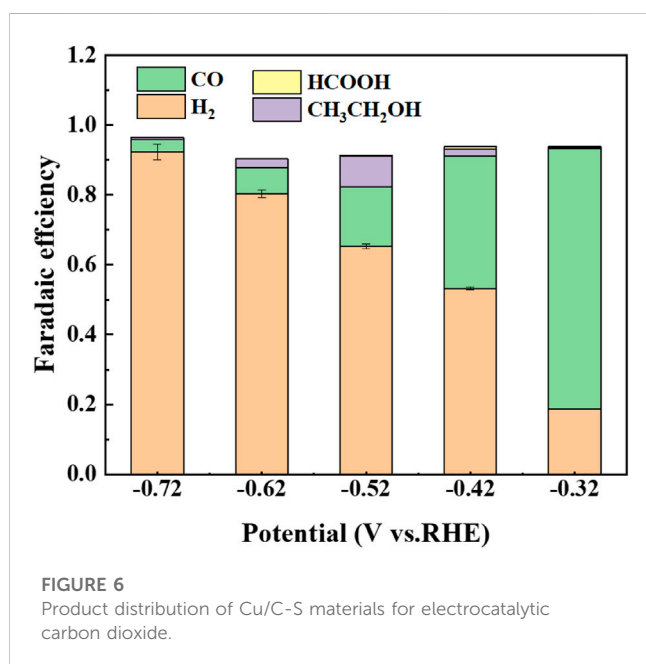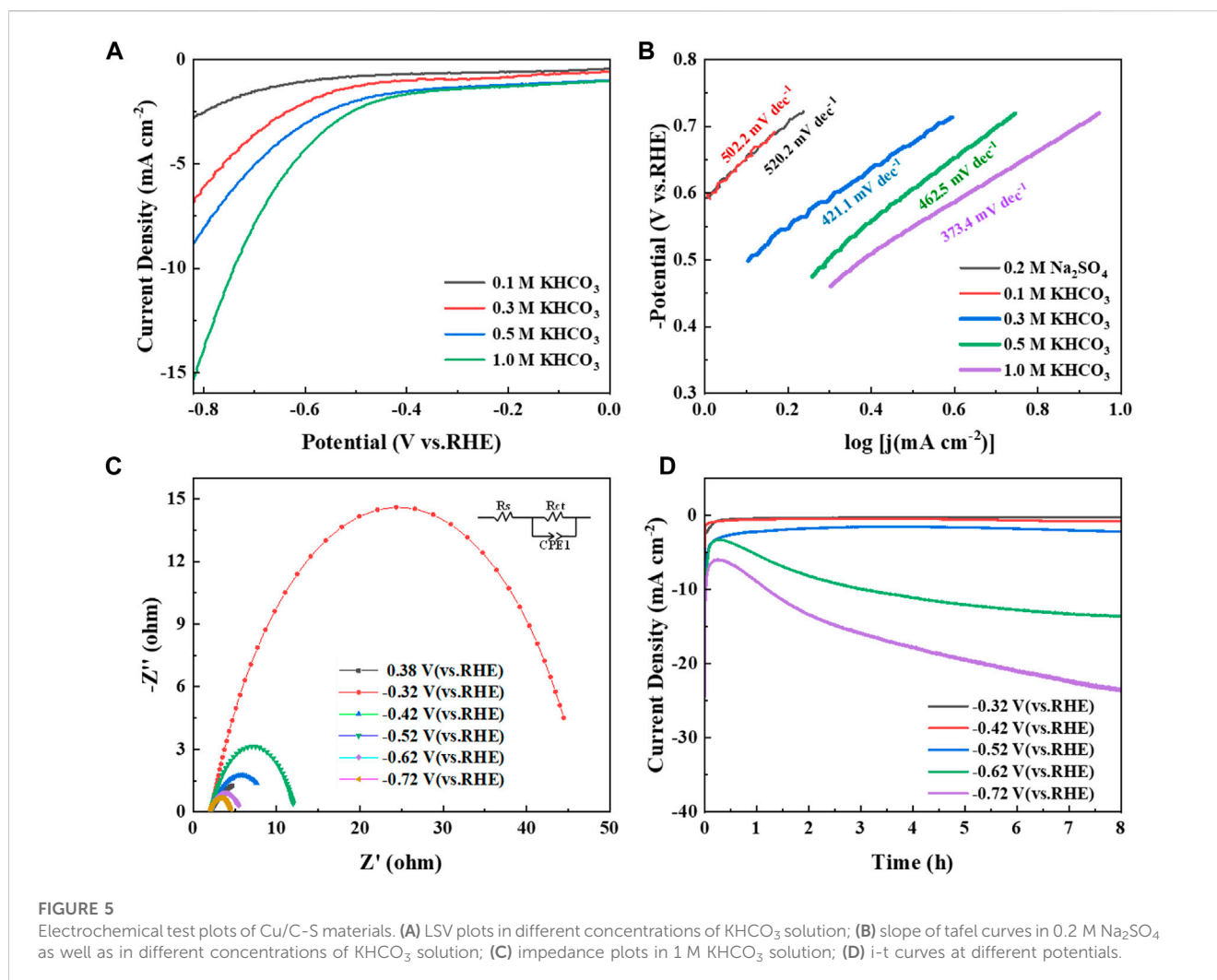
2.2.2 Copper doped modified biochar (Cu/C-S)

The powdered plant tissues after passing through a 40 mesh sieve were added to copper sulfate pentahydrate in a mass ratio of 1:3 (copper: *Elsholtzia Harchowensis*), dissolved in 30 ml of pure water and mixed thoroughly. After stirring with a magnetic stirrer for 2 hours, the beaker was sealed with a sealing film and kept for 24 h. After that, the slurry was dried in the oven at 105℃, and then charred at 700℃ for 90 min at a heating rate of 2℃/min under the nitrogen atmosphere using the tube furnace. The product was mixed with potassium hydroxide powder at a mass ratio of 1:4 (charcoal:

KOH) after cooling and mixed thoroughly, then activated at 700℃ for 90 min. The sample was washed with pure water until neutral, then dried and ground in an agate bowl to obtain copper doped modified biochar (Cu/C-S) as shown in Figure 1.

2.3 Working electrodes

7 mg of catalyst and 100 μl of 5% Nafion solution were mixed in 1 ml of anhydrous ethanol and sonicated for 1 h to make the catalyst dispersed uniformly. Then the mixed slurry was coated on a 1 × 1.5 cm hydrophobic carbon paper in multiple drops with a catalyst loading of 2.4 mg/cm², followed by drying at room temperature.

FIGURE 5
Electrochemical test plots of Cu/C-S materials. **(A)** LSV plots in different concentrations of $KHCO_3$ solution; **(B)** slope of tafel curves in 0.2 M Na_2SO_4 as well as in different concentrations of $KHCO_3$ solution; **(C)** impedance plots in 1 M $KHCO_3$ solution; **(D)** i-t curves at different potentials.

FIGURE 6
Product distribution of Cu/C-S materials for electrocatalytic carbon dioxide.

Before testing, the working electrode was immersed in a 0.2 M Na_2SO_4 solution, and then reduced for 3600 s at a potential of −0.82 V (vs. RHE) for activation.

2.4 Catalyst characterization and testing

2.4.1 Material characterization

The X-ray diffractometer (XRD, Malvern Panalytical Empyrean, Netherlands) was using to determine the crystal structure of the as-prepared catalyst using a Cu target as the radiation source, at a scanning speed of 2°/min from 10° to 80°. The microscopic surface morphology as well as element distribution was observed with a field emission scanning electron microscope (FE-SEM, ZEISS GeminiSEM 300, Germany) equipped with energy dispersive spectrometer (EDS, ZEISS GeminiSEM 300, Germany). For the test with transmission electron microscopy (TEM, JEOL JEM-F200, Japan), the catalysts were firstly dispersed in ethanol solution, and then added dropwisely to a copper grid, followed by photographing with an accelerating voltage of 200 kV. The chemical states of possible elements were analyzed with X-ray
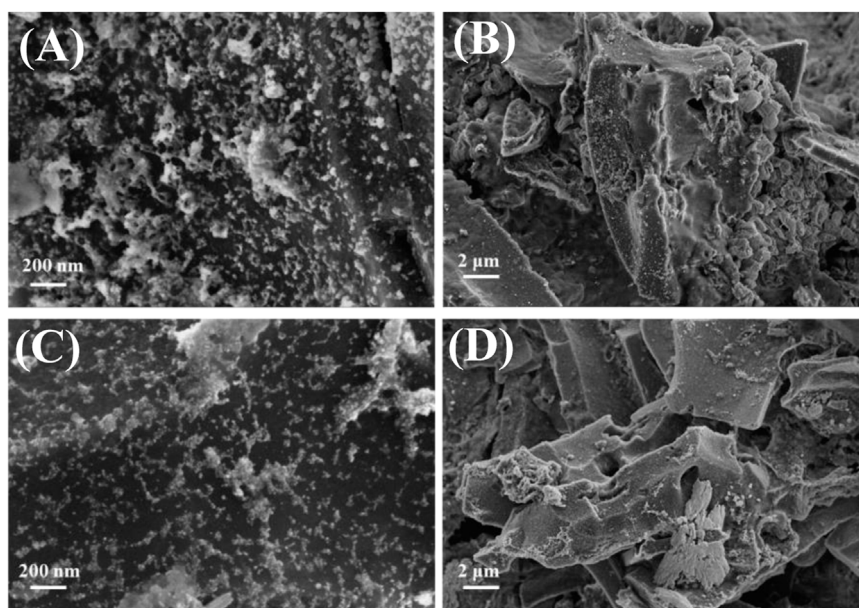
FIGURE 7
SEM images of Cu/C–S material before and after electrochemical testing. **(A, B)** are before the test; **(C, D)** are after the test.
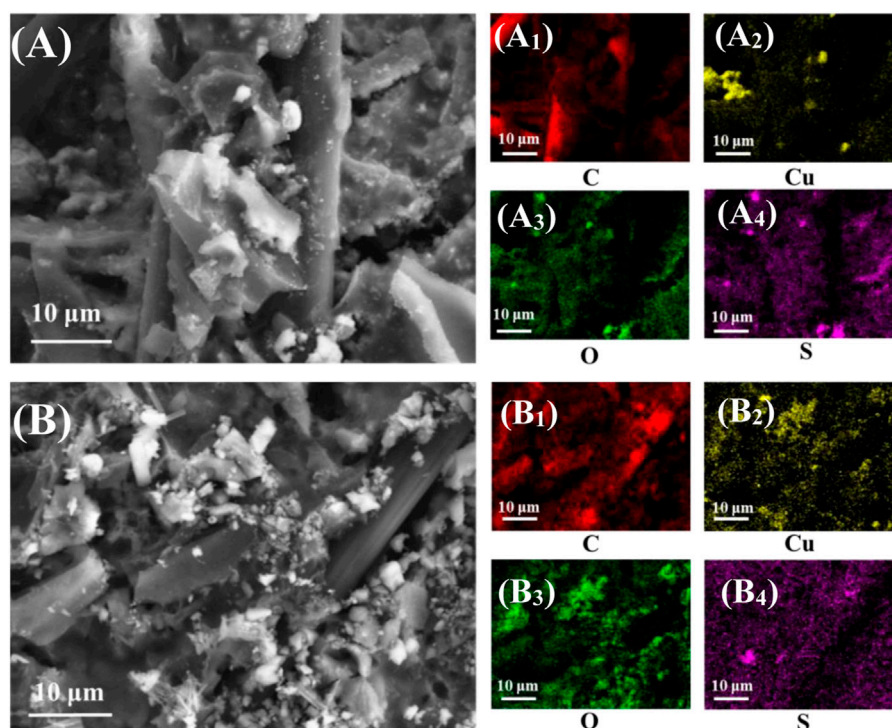
FIGURE 8
EDS-elements mapping of Cu/C–S material before and after electrochemical testing. **(A)** before the test, **(A$_1$–A$_4$)** are elemental spectra; **(B)** after the test, **(B$_1$–B$_4$)** are elemental spectra.

photoelectron spectroscopy (XPS, Thermo Scientific ESCALAB 250Xi, United States) using a monochromatized Al-Kα source (Mono Al-Kα) with hv = 1486.6 eV. The calibration was performed using C 1s with an binding energy of 284.8 eV. Fourier Transform infrared spectroscopy (FT-IR, Thermo Scientific Nicolet iS5, United States) samples were employed to

FIGURE 9
XRD and XPS plots of Cu/C-S materials before and after electrochemical testing. **(A)** XRD plots; **(B)** XPS plots.
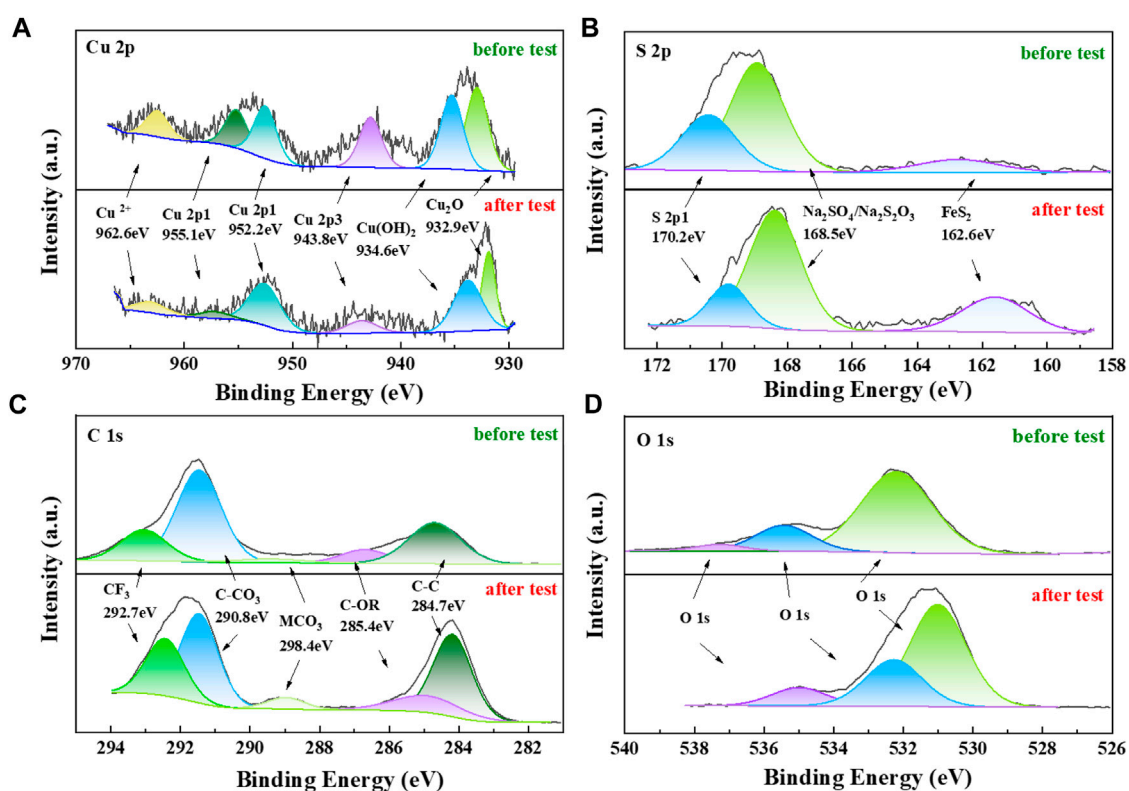
FIGURE 10
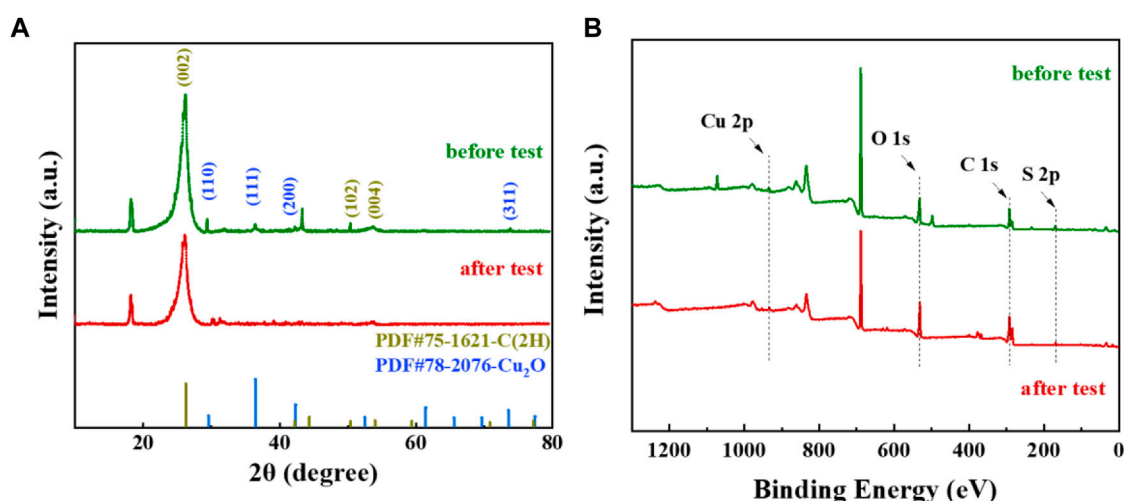XPS fine spectra of Cu/C-S materials before and after electrochemical tests for **(A)** Cu 2p, **(B)** S 2p, **(C)** C 1s, and **(D)** O 1s.

determine the possible functional groups with a range of 400–4,000 cm^{-1}. The automatic specific surface and porosity analyzer (BET, Micromeritics 3Flex, United States) was used to characterize the pore characteristics and surface area with a desorption temperature of 200°C and a degassing time of 8 h.

The specific surface area was calculated by Brunauer Emmett Teller (BET) method, and the pore size characteristics were calculated by Barrett Joyner Halenda (BJH). Determination of metal elements in materials by inductively coupled plasma-mass spectrometry (ICP-MS).

2.4.2 Electrochemical test

The electrocatalytic CO_2RR was carried out in an H-type electrolytic cell with the cathode chamber separated from the anode chamber by a DuPont N-117 proton exchange membrane, and the volume of electrolyte in both chambers was 50 ml. Platinum sheets (2×2 cm) and Ag/AgCl electrodes were used as the counter and reference electrodes, respectively. All electrochemical tests were performed with automatic 95% iR compensation using an electrochemical workstation (CHI660E, Chenhua Instrument Co., Ltd., Shanghai, P. R. China). Before the test, high-purity argon gas (99.999%) was introduced into the cathode chamber for 30 min to exhaust the air from the system, and then high-purity carbon dioxide (99.99%) was introduced for 30 min to saturate the electrolyte with carbon dioxide. The experiment was conducted with a continuous gas flow of carbon dioxide at a rate of 20 ml/min.

In the cathode gas product, hydrogen gas was detected using gas chromatography (GC-9890B, Shanghai Linghua Instrument Co. Ltd., China) with a carrier gas of 99.9% high-purity argon gas, a gas quantitative sampling tube capacity of 1 mL, a thermal conductivity detector (TCD) temperature of 80°C, and a column box temperature of 120°C; Carbon monoxide, methane, and carbon dioxide were chromatographically analyzed (GC 2060, Shanghai Ruimin Instrument Co. Ltd., China) with 99.9% high-purity nitrogen as the carrier gas. The injector temperature was 150°C, the column temperature was 50°C, the hydrogen ion flame detector (FID) temperature was 150°C, and the conversion furnace temperature was 330°C. The liquid products were detected by 1H nuclear magnetic resonance spectrometer (NMR, Bruker 400M, Germany). The electrolyte solution (1000 μL) was sampled for NMR analysis, and DMSO (40 μL) was used as internal standard.

3 Results and discussion

The morphological characteristics of the as-prepared materials were investigated using transmission electron microscopy (TEM), respectively, and the results were shown in Figure 2. Figures 2A, B are TEM images of pristine BC material, while C and D are TEM images of Cu/C-S material. Obviously, both materials were granular in shape with uniform surface distribution and had a good pore structure. Moreover, the particles of Cu/C-S material were darker in the center and brighter at the edges, which indicated that the structure of the catalyst was thicker in the center and decreased gradually at the edges, and it was possible that the black particles on top were copper compounds.

Figure 3A shows the nitrogen adsorption and desorption isotherms of pristine BC and Cu/C-S, both of which belongs to type IV in the IUPAC classification, with H1 hysteresis rings and typical mesoporous adsorption characteristics. According to Brunauer Emmett Teller (BET) theory and Barrett Joyner Halenda (BJH) adsorption model, specific surface area, pore volume and pore size were obtained (Agrafioti et al., 2013), and the results were shown in Supplementary Table S1. The specific surface areas of BC and Cu/C-S were 1202.9 m²/g and 1005.8 m²/g, respectively. The specific surface area and pore volume of the Cu/C-S decreased slightly and the pore size increased slightly after doping with Cu. In addition, as shown in Supplementary Figures S1, S2, the electrochemically active surface area (ECSA) of the material

were determined by using the capacitance method, and the results showed that the ECSA of the Cu/C-S material was 3.4 times larger than that of the BC material, which may be caused by the large number of active sites provided by the surface-loaded elements of Cu/C-S. Figure 3B shows the Fourier Transform infrared spectroscopy (FT-IR) of pristine and Cu/C-S, respectively. The characteristic peak of Cu-O was detected at 600 cm⁻¹ for the Cu/C-S material, indicating the oxide formation of Cu on the surface of $CuSO_4$-modified activated carbon (He et al., 2020). The C-O-C stretching vibration peak near 900–1300 cm⁻¹, the -OH peak appearing at 3449 cm⁻¹ were enhanced for Cu/C-S materials, and the $-CH_3$, $-CH_2$ peak at 2,950–2,860 cm⁻¹ and the C=O, -COOH peak at 1710 cm⁻¹ are approximately unchanged (Fan et al., 2018; Zhu et al., 2019).

Figure 4 shows the linear sweep voltammetry (LSV) curves of the BC and Cu/C-S material electrodes in 0.2 M Na_2SO_4 solution at a scan rate of 10 mV/s. Without $CuSO_4$ modification, the LSV curves of BC material in the atmosphere of argon and CO_2 were shown in Figure 4A, which were basically identical, and the current density was very small (<0.05 mA/cm²). It could be concluded that tiny amount of HER dominated the system, and no significant CO_2RR was observed. This may be due to the limited amount of copper in the directly harvested *Elsholtzia Harchowensis* from the mine, thus making it difficult to observe a significant electrocatalytic CO_2RR reaction. The LSV curves of Cu/C-S materials under argon and CO_2 atmospheres were shown in Figure 4B. The experimental results showed that the onset potential was −0.74 V (@1.0 mA/cm²) under argon atmosphere and −0.61 V (@1.0 mA/cm²) under CO_2 atmosphere. In addition, under the same potential conditions, the current density in CO_2 atmosphere was significantly higher than that in argon saturated system. This may be due to the fact that under the condition of CO_2 purging in Na_2SO_4 solution, not only HER occurred, but also CO_2RR happened at the same time, which contributed to additional current during the electrochemical process. Thus it could be concluded that Cu/C-S had a better electrochemical activity towards CO_2RR.

Figure 5A shows the LSV curves of the Cu/C-S material electrode in different concentrations of $KHCO_3$ solution at a scan rate of 10 mV/s. It can be seen from the figure that when the concentration of $KHCO_3$ solution increased from 0.1 M to 1.0 M, the current density increased continuously and the onset potential of the reaction shifted significantly, which indicated a gradual increase in the electrocatalytic reaction activity. In addition, the tafel curves of the electrocatalytic process at different $KHCO_3$ concentrations were shown in Figure 5B, which showed that the tafel slope in the $KHCO_3$ solution was much smaller than that in the Na_2SO_4 solution, and the Tafel slope gradually decreased as the concentration of the $KHCO_3$ solution increased. The tafel slope in 1.0 M $KHCO_3$ solution was 373.4 mV·dec⁻¹, which indicated a faster growth of current density and better electrocatalytic performance, so the 1.0 M $KHCO_3$ solution was subsequently chosen as the electrolyte solution. Figure 5C shows the impedance test results of Cu/C-S electrocatalytic reduction of CO_2 under different potential conditions, and the results showed that the charge transfer resistance gradually decreased with the negative shift of potential. The material impedance was 7.9 Ω at the open circuit potential of 0.38 V (vs. RHE), 44.9 Ω at −0.32 V (vs.

RHE) and 2.6 Ω at −0.72 V (vs. RHE) (see Supplementary Table S2 for detailed data), which indicated that the Cu/C-S material had good electrocatalytic CO$_2$ reduction activity with low charge transfer resistance for CO$_2$RR. Figure 5D showed the i-t curves at different potentials, which showed a trend of decreasing, then increasing and then stabilizing, with the initial rapid decay of current related to the end of double-layer charging. With the negative shift of potential, the current density gradually increased. The catalyst still has a good catalytic effect after 8 h of stable catalytic CO$_2$ reduction, which indicated that the catalyst had certain stability in practical application.

Figure 6 shows the distribution of final products by using Cu/C-S electrode at different potentials. The main gas phase products were H$_2$ and CO, while the liquid phase products were formic acid and ethanol. CO$_2$ was mainly converted to CO at −0.32 V (vs. RHE), with a high Faraday efficiency of 74.6% and a turnover frequency (TOF) of 107.2 h^{-1}. Faraday efficiency of 8.7% for generating C$_2$ products could be achieved at −0.52 V (vs. RHE). Pristine carbon materials were usually inert for electrochemical CO$_2$RR and the introduction of S elements in the material may provide a large number of active sites and enhance the electrochemical activity of carbon materials (Liu et al., 2015; Asefa, 2016; Zhu et al., 2019). The Faraday efficiency of hydrogen generation was highest at a potential of −0.72 V (vs. RHE). Meanwhile, a trace amount of formate was generated after the reaction (see Supplementary Table S3 for detailed data). *COOH played an important role in the reaction process as a key intermediate in the CO$_2$RR process (*CO$_2^-$ + H$^+$→*COOH). In terms of CO conversion efficiency and TOF of the present material, the present catalyst was superior to most of the catalysts presented in Supplementary Table S4.

In order to continue to investigate the stability of the materials and the changes in the valence and surface functional groups during the reaction, the Cu/C-S materials before and after the electrochemical tests were characterized by SEM-EDS, XRD, XPS, and ICP-MS, respectively. The surface morphologies before and after the electrochemical tests were shown in Figures 7A–D, respectively. It can be seen from the figure that the catalyst loaded on the carbon cloth had a certain laminar structure with a relatively rough surface covered with more spherical particles, and the catalyst was uniformly distributed on the surface of the carbon cloth, which was consistent with the results of TEM, indicating that the black particles aggregated by TEM were compounds of copper. The catalyst morphology was almost unchanged before and after the test, with a slight reduction of particulate matter on the carbon cloth surface, probably due to the shedding of a small amount of material during the reaction. Plants were rich in elements such as C and O, while Cu and S were introduced in the synthesis process. Figures 8A,B showed the EDS-elements mapping scans before and after the test (see Supplementary Figure S4 for EDS layered images). The Cu/C-S material had a relatively uniform distribution of all four elements C, O, Cu, and S before and after the test, and the mass ratio of Cu element is around 7.0% (see Supplementary Figure S5 for the total spectrum of the elemental distribution map). There was a small amount of Cu element aggregation before the test, and the distribution of Cu was more uniform after the test, which better provided active sites CO$_2$RR in the electrochemical process, could possibly be the reason for the gradual increase of current density in the i-t curve at more negative potentials during the electrochemical test.

In order to better understand the crystallographic characteristics of Cu elements on the material surface, the samples were analyzed using XRD, and the test results are shown in Figure 9A. The results showed that the Cu/C-S material had a graphitic carbon as well as Cu$_2$O crystal structure, and the percentage of Cu$_2$O crystals was relatively small. The diffraction peaks at 2θ of 26.2°, 50.3°, 54.0° corresponded to the (002), (102), and (004) crystal planes of graphitic carbon, and the diffraction peaks at 2θ of 29.6°, 36.4°, 42.3°, 73.6° correspond to the (110), (111), (200), and (311) crystal planes of Cu$_2$O (Ren et al., 2015). Several major crystallographic peaks were basically unchanged before and after the reaction, indicating that the material structure remained relatively stable during the electrochemical process. The metallic contents of the as-prepared materials were measured by ICP-MS after microwave digestion. The results confirmed that the Cu/C-S material had Cu, Fe, Zn, Mn, Cr, Sb, Pb and other heavy metals, of which the metal Cu content was 37.9 mg/g as shown in Supplementary Table S5. As for the source of heavy metals such as Fe, Zn, Mn, Cr, Sb, and Pb, it may be due to the presence of these heavy metals in the soil, which were adsorbed and transferred to the plant tissue. Figure 9B shows the XPS full spectrum of the material, which validated the elemental composition as well as the chemical valence state of the sample. The results further demonstrated the presence of C, O, Cu, and S in the material. The fine spectra of C, Cu, S, and O elements (Figure 10) show that the peak position of Cu 2p was basically unchanged before and after the reaction, the element Cu exists mainly in the form of Cu^{II}, Cu^I, and the Cu$_2$O peak at the binding energy of 923.9 eV echoed the FT-IR as well as XRD results, which confirms the existence of Cu$_2$O. The production of Cu$_2$O is first due to the impregnation method, where Cu^{2+} in the solution accumulates in plants through ion exchange or absorption by plant tissue cells. After preparation into electrode materials, the reduction at −0.82 V (vs. RHE) potential for 3600 s resulted in the partial reduction of Cu^{2+} to Cu$_2$O. The peak percentage of Cu$_2$O before and after the reaction is approximately unchanged, which indicates that Cu$_2$O exists in a relatively stable form and can continuously electrocatalytically convert CO$_2$ together with Cu^{2+} in the catalytic process (Wang et al., 2016; Liu et al., 2021). The fine spectrum of S 2p shows a peak of FeS$_2$ at a binding energy of 162.6 eV, which was consistent with the XRD results. It shows that some S element combines with metallic elements to form metal sulfides, while non-metallic anions can provide vacancies for metal cations, which can change the electronic structure of metal cations, thus providing more active site for catalytic reactions (Guo et al., 2022). Due to the high content of element C in the material, many kinds of compounds were generated under high temperature, most of them exist in the form of C-C and C-O, and the peak proportion remains basically unchanged before and after the catalytic reaction. In summary, the XPS results corroborate the SEM results, and the structure and elemental valence of the material remain basically unchanged before and after the long catalytic reaction, with excellent catalyst stability performance.

4 Conclusion

In summary, the carbonaceous materials prepared from *Elsholtzia Harchowensis* had a large specific surface area and

porous structure. The copper sulfate solution modified biochar had excellent electrocatalytic reduction of CO_2 with instantaneous current density up to 15.3 mA/cm^2 at −0.82 V (vs. RHE) electrode potential in 1.0 M KHCO$_3$ solution. When the potential was −0.32 V (vs. RHE), the product CO Faraday efficiency could reach as high as 74.6%. At a potential of −0.52 V (vs. RHE), the C_2^+ product ethanol Faraday efficiency was 8.7%. The modified biochar prepared from *Elsholtzia Harchowensis* can be used as electrode material to realize solid waste utilization and convert carbon dioxide into useful products to achieve environmental protection as well as carbon reduction. This research work can provide new ideas for the utilization of heavy metal-enriched plants and explore the reuse of solid waste to achieve the dual objectives of environmental protection and economy.

Data availability statement

The original contributions presented in the study are included in the article/Supplementary Material, further inquiries can be directed to the corresponding author.

Author contributions

SC, WL, and HT contributed to conception and design of the study. ZM organized the database. HL performed the statistical

Conflict of interest

Publisher's note

Supplementary material

The Supplementary Material for this article can be found online at: https://www.frontiersin.org/articles/10.3389/fchem.2023.1238424/full#supplementary-material

References

Abbas, S.C., Lin, C., Hua, Z., Deng, Q., Huang, H., Ni, Y., et al. (2022). Bamboo-derived carbon material inherently doped with SiC and nitrogen for flexible supercapacitors. *Chem. Eng. J.* 433, 133738. doi:10.1016/J.CEJ.2021.133738

Adrees, M., Ali, S., Rizwan, M., Zia-ur-Rehman, M., Ibrahim, M., Abbas, F., et al. (2015). Mechanisms of silicon-mediated alleviation of heavy metal toxicity in plants: a review. *Ecotoxicol. Environ. Saf.* 119, 186–197. doi:10.1016/j.ecoenv.2015.05.011

Agrafioti, E., Bouras, G., Kalderis, D., and Diamadopoulos, E. (2013). Biochar production by sewage sludge pyrolysis. *J. Anal. Appl. Pyrolysis* 101, 72–78. doi:10.1016/j.jaap.2013.02.010

Alvarenga, P., Gonçalves, A., Fernandes, R., De Varennes, A., Vallini, G., Duarte, E., et al. (2009). Organic residues as immobilizing agents in aided phytostabilization:(I) Effects on soil chemical characteristics. *Chemosphere* 74 (10), 1292–1300. doi:10.1016/j.chemosphere.2008.11.063

Asefa, T. (2016). Metal-free and noble metal-free heteroatom-doped nanostructured carbons as prospective sustainable electrocatalysts. *Accounts Chem. Res.* 49 (9), 1873–1883. doi:10.1021/acs.accounts.6b00317

Barceló, J., and Poschenrieder, C. (2011). Hyperaccumulation of trace elements: From uptake and tolerance mechanisms to litter decomposition; selenium as an example. *Plant soil* 341, 31–35. doi:10.1007/s11104-010-0469-0

Birdja, Y. Y., Pérez-Gallent, E., Figueiredo, M. C., Göttle, A. J., Calle-Vallejo, F., and Koper, M. T. (2019). Advances and challenges in understanding the electrocatalytic conversion of carbon dioxide to fuels. *Nat. Energy* 4 (9), 732–745. doi:10.1038/s41560-019-0450-y

Chen, S., Li, W. H., Jiang, W., Yang, J., Zhu, J., Wang, L., et al. (2022a). MOF encapsulating N-heterocyclic carbene-ligated copper single-atom site catalyst towards efficient methane electrosynthesis. *Angew. Chem. Int. Ed.* 61 (4), 202114450. doi:10.1002/anie.202114450

Chen, S., Wang, B., Zhu, J., Wang, L., Ou, H., Zhang, Z., et al. (2021). Lewis acid site-promoted single-atomic Cu catalyzes electrochemical CO_2 methanation. *Lett.* 21 (17), 7325–7331. doi:10.1021/acs.nanolett.1c02502

Chen, S., Zhang, Z., Jiang, W., Zhang, S., Zhu, J., Wang, L., et al. (2022b). Engineering water molecules activation center on multisite electrocatalysts for enhanced CO_2 methanation. *J. Am. Chem. Soc.* 144 (28), 12807–12815. doi:10.1021/jacs.2c03875

Costentin, C., Passard, G., Robert, M., and Savéant, J.-M. (2014). Ultraefficient homogeneous catalyst for the CO_2-to-CO electrochemical conversion. *Proc. Natl. Acad. Sci.* 111 (42), 14990–14994. doi:10.1073/pnas.1416697111

Costentin, C., Robert, M., and Savéant, J.-M. (2013). Catalysis of the electrochemical reduction of carbon dioxide. *Chem. Soc. Rev.* 42 (6), 2423–2436. doi:10.1039/c2cs35360a

Fan, Q., Sun, J., Chu, L., Cui, L., Quan, G., Yan, J., et al. (2018). Effects of chemical oxidation on surface oxygen-containing functional groups and adsorption behavior of biochar. *Chemosphere* 207, 33–40. doi:10.1016/j.chemosphere.2018.05.044

Franco, F., Rettenmaier, C., Jeon, H. S., and Cuenya, B. R. (2020). Transition metal-based catalysts for the electrochemical CO_2 reduction: From atoms and molecules to nanostructured materials. *Chem. Soc. Rev.* 49 (19), 6884–6946. doi:10.1039/d0cs00835d

Fu, H. Q., Liu, J., Bedford, N. M., Wang, Y., Sun, J. W., Zou, Y., et al. (2022). Synergistic Cr_2O_3@ Ag heterostructure enhanced electrocatalytic CO_2 reduction to CO. *Adv. Mater.* 34 (29), 2202854. doi:10.1002/adma.202202854

Fu, Y., Sun, D., Chen, Y., Huang, R., Ding, Z., Fu, X., et al. (2012). An amine-functionalized titanium metal-organic framework photocatalyst with visible-light-induced activity for CO_2 reduction. *Angew. Chem. Int. Ed.* 51 (14), 3420–3423. doi:10.1002/ange.201108357

Grandlic, C. J., Palmer, M. W., and Maier, R. M. (2009). Optimization of plant growth-promoting bacteria-assisted phytostabilization of mine tailings. *Soil Biol. Biochem.* 41 (8), 1734–1740. doi:10.1016/j.soilbio.2009.05.017

Guo, C., Guo, Y., Shi, Y., Lan, X., Wang, Y., Yu, Y., et al. (2022). Electrocatalytic reduction of CO_2 to ethanol at close to theoretical potential via engineering abundant electron-donating Cuδ+ species. *Angew. Chem.* 134 (32), 202205909. doi:10.1002/anie.202205909

Habisreutinger, S. N., Schmidt-Mende, L., and Stolarczyk, J. K. (2013). Photocatalytic reduction of CO_2 on TiO_2 and other semiconductors. *Angew. Chem. Int. Ed.* 52 (29), 7372–7408. doi:10.1002/anie.201207199

He, W., Liberman, I., Rozenberg, I., Ifraemov, R., and Hod, I. (2020). Electrochemically driven cation exchange enables the rational design of active CO_2 reduction electrocatalysts. *Angew. Chem.* 132 (21), 8339–8346. doi:10.1002/ange.202000545

Hori, Y. i. (2008). Electrochemical CO_2 reduction on metal electrodes, *Modern Aspects of Electrochemistry*, 42. Springer, New York, NY, USA, 89–189. doi:10.1007/978-0-387-49489-0_3

Hori, Y., Kikuchi, K., Murata, A., and Suzuki, S. J. C. L. (1986). Production of methane and ethylene in electrochemical reduction of carbon dioxide at copper electrode in

aqueous hydrogencarbonate solution. *Chem. Lett.* 15 (6), 897–898. doi:10.1246/cl.1986.897

Jian, L., Changyong, H., Ying, T., and Huaiying, Y. (2004). Research on soil microbial characteristics of soil-Elsholtzia harchowensis system in copper mine tailings. *Acta Pedol. Sin.* 41 (1), 120–125. doi:10.4028/www.scientific.net/AMR.919-921.2174

Jiang, L. Y., Yang, X., and He, Z. (2004). Growth response and phytoextraction of copper at different levels in soils by Elsholtzia splendens. *Chemosphere* 55 (9), 1179–1187. doi:10.1016/j.chemosphere.2004.01.026

Li, Z.-X., Wei, X.-Y., Yang, Z., Zhang, M., Meng, X.-L., Niu, S., et al. (2020). Highly selective hydrogenation of furfural to furan-2-ylmethanol over zeolitic imidazolate frameworks-67-templated magnetic Cu–Co/C. *Catal. Lett.* 150, 178–184. doi:10.1007/s10562-019-02925-1

Liu, D., Xu, G., Fan, B., and Wang, H. (2022). *In situ* encapsulation of abundant WP/Ni$_2$P heterointerfaces in N, P co-doped two-dimensional carbon frameworks for boosting hydrogen evolution electrocatalysis. *Dalton Trans.* 51 (46), 17911–17918. doi:10.1039/D2DT02606F

Liu, D., Xu, G., Yang, H., Wang, H., and Xia, B. Y. (2023). Rational design of transition metal phosphide-based electrocatalysts for hydrogen evolution. *Adv. Funct. Mater.* 33 (7), 2208358. doi:10.1002/adfm.202208358

Liu, G., Zheng, F., Li, J., Zeng, G., Ye, Y., Larson, D. M., et al. (2021). Investigation and mitigation of degradation mechanisms in Cu$_2$O photoelectrodes for CO$_2$ reduction to ethylene. *Nat. Energy* 6 (12), 1124–1132. doi:10.1038/S41560-021-00927-1

Liu, J., Song, P., Ning, Z., and Xu, W. (2015). Recent advances in heteroatom-doped metal-free electrocatalysts for highly efficient oxygen reduction reaction. *Electrocatalysis* 6, 132–147. doi:10.1007/s12678-014-0243-9

Liu, S., Yang, H., Huang, X., Liu, L., Cai, W., Gao, J., et al. (2018). Identifying active sites of nitrogen-doped carbon materials for the CO$_2$ reduction reaction. *Adv. Funct. Mater.* 28 (21), 1800499. doi:10.1002/adfm.201800499

Ma, W., Xie, S., Zhang, X.-G., Sun, F., Kang, J., Jiang, Z., et al. (2019). Promoting electrocatalytic CO$_2$ reduction to formate via sulfur-boosting water activation on indium surfaces. *Nat. Commun.* 10 (1), 892. doi:10.1038/s41467-019-08805-x

Mac Dowell, N., Fennell, P. S., Shah, N., and Maitland, G. C. (2017). The role of CO$_2$ capture and utilization in mitigating climate change. *Nat. Clim. change* 7 (4), 243–249. doi:10.1038/nclimate3231

Markewitz, P., Kuckshinrichs, W., Leitner, W., Linssen, J., Zapp, P., Bongartz, R., et al. (2012). Worldwide innovations in the development of carbon capture technologies and the utilization of CO$_2$. *Energy & Environ. Sci.* 5 (6), 7281–7305. doi:10.1039/C2EE03403D

Nitopi, S., Bertheussen, E., Scott, S. B., Liu, X., Engstfeld, A. K., Horch, S., et al. (2019). Progress and perspectives of electrochemical CO$_2$ reduction on copper in aqueous electrolyte. *Chem. Rev.* 119 (12), 7610–7672. doi:10.1021/acs.chemrev.8b00705

Niu, H., Xia, C., Huang, L., Zaman, S., Maiyalagan, T., Guo, W., et al. (2022). Rational design and synthesis of one-dimensional platinum-based nanostructures for oxygen-reduction electrocatalysis. *Chin. J. Catal.* 43 (6), 1459–1472. doi:10.1016/S1872-2067(21)63862-7

Qiao, J., Liu, Y., Hong, F., and Zhang, J. (2014). A review of catalysts for the electroreduction of carbon dioxide to produce low-carbon fuels. *Chem. Soc. Rev.* 43 (2), 631–675. doi:10.1039/C3CS60323G

Rascio, N., and Navari-Izzo, F. (2011). Heavy metal hyperaccumulating plants: How and why do they do it? And what makes them so interesting?. *Plant Sci.* 180 (2), 169–181. doi:10.1016/j.plantsci.2010.08.016

Ren, D., Deng, Y., Handoko, A. D., Chen, C. S., Malkhandi, S., and Yeo, B. S. (2015). Selective electrochemical reduction of carbon dioxide to ethylene and ethanol on copper (I) oxide catalysts. *Acs Catal.* 5 (5), 2814–2821. doi:10.1021/cs502128q

Ross, M. B., De Luna, P., Li, Y., Dinh, C.-T., Kim, D., Yang, P., et al. (2019). Designing materials for electrochemical carbon dioxide recycling. *Nat. Catal.* 2 (8), 648–658. doi:10.1038/s41929-019-0306-7

Sarwar, N., Imran, M., Shaheen, M. R., Ishaque, W., Kamran, M. A., Matloob, A., et al. (2017). Phytoremediation strategies for soils contaminated with heavy metals: Modifications and future perspectives. *Chemosphere* 171, 710–721. doi:10.1016/j.chemosphere.2016.12.116

Song, J., Zhao, F.-J., Luo, Y.-M., McGrath, S. P., and Zhang, H. (2003). Copper uptake by Elsholtzia splendens and Silene vulgaris and assessment of copper phytoavailability in contaminated soils. *Environ. Pollut.* 128 (3), 307–315. doi:10.1016/j.envpol.2003.09.019

Sun, J., Qiu, X., Wang, Z., Peng, Z., Jiang, L., Li, G., et al. (2021). An efficient oxygen reduction catalyst for Zn-air battery: Cobalt nanoparticles encapsulated in 3D nitrogen-doped porous carbon networks derived from fish scales. *ChemCatChem* 13 (10), 2474–2482. doi:10.1002/cctc.202001855

Sun, X., Gao, X., Chen, J., Wang, X., Chang, H., Li, B., et al. (2020). Ultrasmall Ru nanoparticles highly dispersed on sulfur-doped graphene for HER with high electrocatalytic performance. *ACS Appl. Mater. Interfaces* 12 (43), 48591–48597. doi:10.1021/acsami.0c14170

Tang, C., Zheng, Y., Jaroniec, M., and Qiao, S. Z. (2021). Electrocatalytic refinery for sustainable production of fuels and chemicals. *Angew. Chem. Int. Ed.* 60 (36), 19724–19742. doi:10.1002/ANGE.202101522

Wang, H., Jia, J., Song, P., Wang, Q., Li, D., Min, S., et al. (2017). Efficient electrocatalytic reduction of CO$_2$ by nitrogen-doped nanoporous carbon/carbon nanotube membranes: A step towards the electrochemical CO$_2$ refinery. *Angew. Chem.* 129 (27), 7955–7960. doi:10.1002/ange.201703720

Wang, H., Qiu, X., Wang, W., Jiang, L., and Liu, H. (2019). Iron sulfide nanoparticles embedded into a nitrogen and sulfur co-doped carbon sphere as a highly active oxygen reduction electrocatalyst. *Front. Chem.* 7, 855. doi:10.3389/fchem.2019.00855

Wang, H., Sun, J., Wang, J., Jiang, L., and Liu, H. (2021). Green synthesis of nitrogen and fluorine co-doped porous carbons from sustainable coconut shells as an advanced synergistic electrocatalyst for oxygen reduction. *J. Mater. Res. Technol.* 13, 962–970. doi:10.1016/j.jmrt.2021.05.048

Wang, J., Li, Z., Wu, Y., and Li, Y. (2018). Fabrication of single-atom catalysts with precise structure and high metal loading. *Adv. Mater.* 30 (48), 1801649. doi:10.1002/adma.201801649

Wang, W., Wang, S., Ma, X., and Gong, J. (2011). Recent advances in catalytic hydrogenation of carbon dioxide. *Chem. Soc. Rev.* 40 (7), 3703–3727. doi:10.1039/c1cs15008a

Wang, Z.-L., Li, C., and Yamauchi, Y. (2016). Nanostructured nonprecious metal catalysts for electrochemical reduction of carbon dioxide. *Today* 11 (3), 373–391. doi:10.1016/j.nantod.2016.05.007

Zhang, J., Zhao, Y., Chen, C., Huang, Y.-C., Dong, C.-L., Chen, C.-J., et al. (2019). Tuning the coordination environment in single-atom catalysts to achieve highly efficient oxygen reduction reactions. *J. Am. Chem. Soc.* 141 (51), 20118–20126. doi:10.1021/jacs.9b09352

Zhang, Z., Zhu, J., Chen, S., Sun, W., and Wang, D. (2023). Liquid fluxional Ga single atom catalysts for efficient electrochemical CO$_2$ reduction. *Angew. Chem.* 135 (3), 202215136. doi:10.1002/anie.202215136

Zheng, T., Jiang, K., and Wang, H. (2018). Recent advances in electrochemical CO$_2$-to-CO conversion on heterogeneous catalysts. *Adv. Mater.* 30 (48), 1802066. doi:10.1002/adma.201802066

Zheng, W., Wang, Y., Shuai, L., Wang, X., He, F., Lei, C., et al. (2021). Highly boosted reaction kinetics in carbon dioxide electroreduction by surface-introduced electronegative dopants. *Adv. Funct. Mater.* 31 (15), 2008146. doi:10.1002/ADFM.202008146

Zhu, K., Wang, X., Geng, M., Chen, D., Lin, H., and Zhang, H. (2019). Catalytic oxidation of clofibric acid by peroxydisulfate activated with wood-based biochar: Effect of biochar pyrolysis temperature, performance and mechanism. *Chem. Eng. J.* 374, 1253–1263. doi:10.1016/j.cej.2019.06.006

Zhu, W., Michalsky, R., Metin, O. n., Lv, H., Guo, S., Wright, C. J., et al. (2013). Monodisperse Au nanoparticles for selective electrocatalytic reduction of CO$_2$ to CO. *J. Am. Chem. Soc.* 135 (45), 16833–16836. doi:10.1021/ja409445p